Virology 527 (2019) 159–168

Contents lists available at ScienceDirect

Virology

journal homepage: www.elsevier.com/locate/virology

A method for analyzing the composition of viral nucleoprotein complexes, produced by heterologous expression in bacteria

Melissa N. Webby[a,1], Matthew P. Sullivan[b], Kavestri M. Yegambaram[a], Mazdak Radjainia[a,2], Jeremy R. Keown[a,3], Richard L. Kingston[a,*]

[a] School of Biological Sciences, University of Auckland, Auckland, New Zealand
[b] School of Chemical Sciences, University of Auckland, Auckland, New Zealand

ARTICLE INFO

Keywords:
Paramyxovirus
Negative-sense ssRNA viruses
Nucleocapsid
Protein and Nucleic acid quantification
Electron Microscopy
Analytical Ultracentrifugation
UV absorbance spectroscopy
Circular dichroism spectroscopy
Biuret assay
Inductively coupled plasma mass spectrometry

ABSTRACT

Viral genomes are protected and organized by virally encoded packaging proteins. Heterologous production of these proteins often results in formation of particles resembling the authentic viral capsid or nucleocapsid, with cellular nucleic acids packaged in place of the viral genome. Quantifying the total protein and nucleic acid content of particle preparations is a recurrent biochemical problem. We describe a method for resolving this problem, developed when characterizing particles resembling the Menangle Virus nucleocapsid. The protein content was quantified using the biuret assay, which is largely independent of amino acid composition. Bound nucleic acids were quantified by determining the phosphorus content, using inductively coupled plasma mass spectrometry. Estimates for the amount of RNA packaged within the particles were consistent with the structurally-characterized packaging mechanism. For a bacterially-produced nucleoprotein complex, phosphorus usually provides a unique elemental marker of bound nucleic acids, hence this method of analysis should be routinely applicable.

1. Introduction

The production of virus–like-particles (VLPs) and nucleocapsid-like particles (NLPs) using heterologous expression systems (reviewed in (Zeltins, 2013)) has been critical in exploring the basic molecular biology of viruses. VLP and NLP production is also central to vaccinology (Bárcena and Blanco, 2013; Roldão et al., 2010) and nanotechnology (Bittner et al., 2013; Carrico and Kirshenbaum, 2009; Narayanan and Han, 2017). VLPs and NLPs effectively mimic the structures associated with authentic virions, but lack the viral genome, and are hence non-infectious.

Heterologous production of viral capsid and nucleocapsid proteins can result in the production of "empty" particles which do not package nucleic acids. However, in many cases particles will package cellular nucleic acids in place of the viral genome. The total protein and nucleic acid content of particle preparations needs to be estimated to gain insight into the packaging process, and to enable quantitative biophysical analysis. This is the problem addressed in this paper. We do not consider the problem of determining the size or sequence of the packaged nucleic acids, which has been discussed elsewhere (Ferrer et al., 2016).

Estimates of protein content can be related to the particle concentration, where the particles are of fixed size. Estimates of both protein and nucleic acid content can be used to calculate the mean amount of nucleic acid packaged per particle or per protein subunit. Even high-resolution imaging of VLPs and NLPs, using methods such as X-ray crystallography and cryo-electron microscopy, may not yield this information. This is because the nucleic acids bound within the particles are compositionally heterogeneous, and the packaged nucleic acids may not conform to the capsid symmetry (Cuervo et al., 2013; Schneemann, 2006), complicating image reconstruction and interpretation.

One approach to quantification is to physically separate proteins and nucleic acids, making it easier to estimate one or both components using standard procedures. The drawback of this approach is that material may be lost during the separation step. Compositional analysis of intact particles is therefore preferable. Mass measurements on individual particles using scanning transmission electron microscopy can provide considerable insight into nucleic acid packaging (Briggs et al.,

* Corresponding author.
E-mail address: rl.kingston@auckland.ac.nz (R.L. Kingston).
[1] Present addres: Department of Biochemistry, University of Oxford, Oxford, UK.
[2] Present addres: Thermo Fisher Scientific, Eindhoven, the Netherlands.
[3] Present addres: Division of Structural Biology, University of Oxford, Oxford, UK.

https://doi.org/10.1016/j.virol.2018.11.013
Received 4 August 2018; Received in revised form 23 October 2018; Accepted 22 November 2018
Available online 04 December 2018
0042-6822/

2004; Müller et al., 2011; Thomas et al., 1994), however this requires access to highly specialized instrumentation.

UV absorption spectroscopy is the most widely used technique for the estimation of protein and nucleic acid concentration. However, the UV absorbance spectra of nucleoprotein complexes are complicated by the overlapping absorption from protein and nucleic acid chromophores, in addition to the complex absorption of the nucleobases themselves. Protein absorption in the near UV region ($\lambda > 240$ nm) is dominated by the phenol and indole groups of tyrosine and tryptophan. Their spectral contributions are essentially additive, and only weakly dependent on the environment (Gill et al., 1989; Pace et al., 1995). In contrast, absorption by the nucleobases in this region is not additive, depending strongly on interactions between nucleotides, and hence the base stacking arrangement (Bloomfield et al., 2000). In addition, the exact composition of the nucleic acids packaged in VLPs and NLPs is unknown.

Despite these difficulties, a variety of procedures have been developed for estimating the protein and nucleic acid content of nucleoprotein complexes from UV absorbance measurements. Porterfield and Zlotnick detail a procedure for estimating the protein and RNA content of viral particles, assuming a mean value for the molar absorption coefficient of the RNA bases (Porterfield and Zlotnick, 2010). Validated for several icosahedral capsids, the applicability of the method rests on the absence of persistent RNA structure and base stacking in the particle – conditions which are often not satisfied for helical viruses and nucleocapsids (Ruigrok et al., 2011; Stubbs and Kendall, 2011). An earlier approach for protein determination in nucleoprotein complexes is based on the measurement of absorbance at several wavelengths that bracket the nucleic acid absorbance minimum at ~230 nm (Groves et al., 1968). The two wavelengths are selected so that nucleic acid absorbance is the same at each, providing a basis for estimating the protein contribution. However, the "iso-absorbing" wavelengths for nucleic acids will again depend on both their composition and structure, hence this method is also approximate. Finally, analysis of spectral derivatives has been used to determine the composition of protein and nucleic acid mixtures (Mach et al., 1992; Wilson et al., 1989). However, while the relative contribution of protein and nucleic acid is reweighted in spectral derivatives, the features due to each component remain poorly resolved, and this method has not been widely adopted.

We have developed an alternative method for analyzing the composition of nucleoprotein complexes that can be readily applied to particles containing structured nucleic acids. To quantify the protein, we use the biuret assay, a classical but now rarely used biochemical tool. To quantify the nucleic acid, we determine the phosphorus content, using inductively coupled plasma mass spectrometry (ICP-MS). For a pure nucleoprotein complex produced in bacteria, nucleic acids are likely to provide the sole source of phosphorus in the sample.

We developed the procedure while characterizing Menangle Virus NLPs. Menangle Virus is a recently emergent zoonotic paramyxovirus, closely related to the human mumps virus (Bowden et al., 2001). We purified Menangle Virus NLPs corresponding to a single turn of the viral nucleocapsid and performed biophysical analysis to investigate particle homogeneity. Measurement of protein and nucleic acid content in the particle preparations returned estimates for the amount of encapsidated RNA that are consistent with the structurally-characterized mechanism for RNA packaging. This validates the procedure, which can be applied to particles with unknown protein and nucleic acid stoichiometry. As VLPs and NLPs are often produced in bacteria, the quantification method has general utility.

2. Materials and methods

2.1. Heterologous production of the N protein from Menangle Virus in bacteria

A bacterial plasmid for expressing the full length MenV N protein (519 amino acids; NCBI Accession ID AF326114; UniProt Accession ID Q91MK3), fused to a C-terminal polyhistidine tag, has been previously described (Yegambaram et al., 2013). This plasmid was modified to express an untagged protein, by introducing a stop codon immediately following the N protein coding sequence. The plasmid was transformed into *E. coli* BL21 Star™ (DE3) cells (Strategene). Cultures of transformed bacteria (0.75 L) were grown at 37 °C with shaking, in LB media supplemented with 1% (v/v) glycerol (Losen et al., 2004) and kanamycin (25 mg/L). When the apparent absorbance at 600 nm was ~0.6, protein production was induced by addition of 0.5 mM IPTG. Cultures were subsequently maintained at 18 °C for 5 h prior to harvesting via centrifugation.

2.2. Isolation of nucleocapsid-like particles

Pelleted cells were re-suspended at 4 °C in 5 mL of lysis buffer (12.5 mM MOPS/KOH pH 7.0, 150 mM NaCl, 0.5 mM tetra-sodium EDTA, 0.25 mM TCEP.HCl and 5%(v/v) glycerol), per g of wet cell mass. The lysis buffer was supplemented with a cOmplete mini protease inhibitor cocktail tablet (Roche) and 0.1 mg/mL RNase A (Roche). Following lysis by sonication (4 °C, Qsonica Q700), the insoluble material was pelleted by high-speed centrifugation. A two-step ammonium sulphate fractionation was then performed; the first step removing cellular contaminants, and the second step isolating the majority of the N protein. In the first step, solid ammonium sulphate was added to the supernatent to a concentration of 0.10 g/mL (18% saturation (Duong-Ly and Gabelli, 2014; Englard and Seifter, 1990)), and the solution mixed at room temperature for 8 min. Precipitated material was pelleted by centrifugation (4 °C) and discarded. In the second step, additional ammonium sulphate was added, to achieve a final concentration of 0.17 g/mL (30% saturation). Following mixing and centrifugation, the pelleted material was re-suspended in SEC buffer (12.5 mM MOPS/KOH pH 7.0, 150 mM NaCl, 0.5 mM tetra-sodium EDTA, 0.25 mM TCEP.HCl and 0.5 mM NaN_3), employing 0.5 mL buffer per g of originating wet cell mass.

The solution was filtered (0.2 μm cellulose acetate membrane filter, Sartorius) and loaded onto a Sephacryl S-500 s column, attached to an AKTA purifier system. The void volume of the column was determined using nanosphere beads (Thermo Fisher Scientific) (Reynolds et al., 1983), and the internal volume of the gel matrix subsequently determined from the elution volume of tyrosine. Isocratic elution of protein at 20 °C with a flow rate of 0.8 mL/min gave adequate separation of rings from both smaller assemblages and larger helical filaments (Fig. S1). Fractions containing N protein were identified by SDS-PAGE, and filtered samples analysed by dynamic laser light scattering to identify the average hydrodynamic radius. Fractions across the major peak in the chromatogram (Fig. S1) with an average hydrodynamic radius < 14 nm were pooled, and subject to anion exchange chromatography. The NLPs were bound to Q sepharose HP resin (GE Healthcare) equilibrated with low salt buffer (12.5 mM Tris/HCl pH 8.5, 50 mM NaCl, 0.5 mM tetrasodium EDTA and 0.25 mM TCEP.HCl) and eluted using a linear 50–1000 mM NaCl gradient. The NLPs eluted in a single major peak at 0.6 M NaCl. Pooled fractions, selected based on average hydrodynamic radius as above, were spin concentrated (30,000 MWCO, Amicon) and dialysed overnight (50,000 MWCO cellulose acetate membrane, Harvard Apparatus) into a standard storage buffer (12.5 mM MOPS/KOH pH 7.0, 150 mM NaCl, 0.25 mM TCEP.HCl). The resulting NLP preparation contained no significant protein contaminants, as assessed by SDS-PAGE coupled with Colloidal Coomassie staining (Candiano et al., 2004) (Fig. S2).

2.3. Biuret assay for determination of total protein concentration

The total protein concentration in the NLP preparation was determined using the biuret assay. Reagents were as detailed by Honn and Chavin (Honn and Chavin, 1975), but with 10x less Potassium Iodide

incorporated (Gornall and Manolis, 1977; Gornall et al., 1949). The stock reagents A (30 g/L $CuSO_4{\cdot}5H_2O$, 90 g/L sodium potassium tartrate, 1 g/L KI and 1.6 g/L NaOH) and B (8 g/L NaOH and 1 g/L KI) were mixed in 1:4 ratio to prepare the working reagent. Freshly prepared working reagent (200 µL) was added to protein-containing solutions (50 µL, in standard storage buffer) and samples were incubated for 30 min at room temperature, to allow the reaction to proceed to completion. Absorbance at 550 nm was measured on a Cary 4000 spectrometer (Varian), relative to a negative control (storage buffer plus reagent). A standard curve, generated from three technical replicate measurements of hen egg white lysozyme (HEWL), enabled estimation of the unknown protein concentration in the NLP preparations (Fig. S3).

To make the standards, crystalline HEWL (Merck) was reconstituted in standard storage buffer to make a stock solution of ~ 10 mg/mL. The exact concentration of HEWL was determined from absorbance at 280 nm, assuming a molar absorption coefficient of 36230 M^{-1} cm^{-1} (Bruzzesi et al., 1965) and molar mass of 14309 g/mol. Protein concentration standards were prepared from the stock HEWL solution by serial dilution. Absorbance versus concentration data was fit with a linear function having zero intercept. Linear fits used for estimation of unknown protein concentrations had $R^2 > 0.98$.

2.4. Electron microscopy

Images were acquired on FEI Tecnai 12 TEM microscope equipped with a LaB_6 filament and operated at 120 kV. For Cryo-electron microscopy (Cryo-EM) the NLP preparation (0.5 mg/mL total protein concentration) was applied to holey carbon grids (QUANTIFOIL® R 2/2) that had been glow discharged with N-amylamine present (Dubochet et al., 1971). Samples were flash frozen in liquid ethane using a vitrobot (Mark VI, FEI) set at 3 s blot time, 4 °C and 100% humidity.

Images were recorded at a nominal magnification of 50,000× on photographic film (Kodak SO-163), which was developed according to manufacturer's instructions. Selected images were digitized using a Nikon LS-9000 film scanner with a raster step size of 7.81 µm corresponding to 1.575 Å on the specimen. The Eman2 software package (Tang et al., 2007) was used to perform automatic determination of the contrast transfer function (CTF) parameters (e2ctf). Following CTF correction, ~9000 particle images were boxed (box size of 22.4 nm) and sorted into 24 classes using reference-free class averaging (e2refine2d).

2.5. Dynamic laser light scattering

Dynamic light scattering (DLS) was used to estimate the size of species throughout purification. Samples were spin filtered (0.2 µm) and subjected to high-speed centrifugation prior to measurement. DLS measurements were made at 831.1 nm and 20 °C using a DynaPro Titan (Wyatt Technology). Intensity autocorrelation functions (ACFs) were subject to cumulants analysis (Frisken, 2001; Koppel, 1972) using both laboratory and commercial software (Dynamics, Wyatt Technology), to estimate both the Z-average diffusion coefficient of the scattering species (Finsy and De Jaeger, 1991) and the polydispersity. From the Z-average diffusion coefficient, the harmonic Z-average hydrodynamic radius (Finsy and De Jaeger, 1991) was computed using the Stokes-Einstein equation. DLS measurements on purified NLP preparations were made at multiple concentrations (0.03-0.5 mg/mL total protein concentration), and the results linearly extrapolated to infinite dilution, allowing estimation of the true diffusion coefficient of the NLPs (Harding, 1994) (Fig. S4).

The expected hydrodynamic radius of the NLPs was approximated using estimated values for a circular cylinder of length (L) and diameter (d) (Hansen, 2004), with dimensions appropriate for either a 13-membered ring, or two stacked rings (Alayyoubi et al., 2015).

2.6. Analytical ultracentrifugation

Sedimentation Velocity analytical ultracentrifugation (AUC) experiments were conducted at 20 °C in a Beckman Coulter model XL-I equipped with absorbance optics. The NLP sample and reference solutions were loaded into a Beckman Coulter eight-compartment An-50 Ti rotor and centrifuged at 14,000 rpm, measuring absorbance at 280 nm. Continuous sedimentation coefficient distributions c(s) and molar mass distributions c(M) were estimated from the data by direct modelling of the concentration profiles, as implemented in the program SEDFIT (Dam and Schuck, 2004; Schuck, 2000). For analysis, it was assumed that the species present were not interconverting on the experimental timescale, and that all species present could be described by a single weight-averaged frictional ratio, estimated during fitting. SEDNTERP (Laue et al., 1992) was used to calculate the buffer density (1.005 g/mL) and viscosity (0.01020 cP) as well as the partial specific volume ($\bar{\nu}$) of the N protein (0.722 cm^3/g). The partial specific volume of RNA was taken to be 0.54 cm^3/g (Durchschlag, 1989). The partial specific volume of the NLPs was calculated according to:

$$\bar{\nu}_{NLP} = f_{protein}\,\bar{\nu}_{protein} + f_{RNA}\,\bar{\nu}_{RNA}$$

Where $f_{protein}$ and f_{RNA} are the weight fractions of each component in the complex. On a per subunit basis, the molar mass of the protein component, determined from the amino acid sequence is 58915 g/mol, while the molar mass of the RNA component was taken as 2037 (= 6 × 339.5) g/mol. Here we are assuming that the average molar mass of an RNA monophosphate base is 339.5 g/mol and six nucleotides are bound per N protein monomer, based on the "rule of 6" (Calain and Roux, 1993; Kolakofsky et al., 1998), prior structural analysis of the rubulaviral nucleocapsid (Alayyoubi et al., 2015), and our own experimental analysis of RNA content (vide infra). Under this assumption, the partial specific volume of the NLPs was estimated as 0.716 cm^3/g and input into SEDFIT for modelling.

2.7. UV absorption and circular dichroism spectroscopy

Ultraviolet (UV)-Visible absorbance spectra (200–800 nm) were collected at a temperature of 20 °C using a Cary 4000 spectrophotometer (Varian) on NLPs (0.5 mg/mL total N protein concentration) in 20 mM Na_2HPO_4/NaH_2PO_4 pH 7.0, 50 mM NaCl and 0.25 mM TCEP.HCl. Because of their large size, the NLPs can produce measurable light scattering in the ultraviolet region (Harding, 1986). To evaluate and correct for this, a function of form $a_0 + a_1 / \lambda^b$ was fitted to the NLP absorbance data at wavelengths > 360 nm, where only light scattering effects should be present (cf. (Camerini-Otero and Day, 1978)). The fit scattering function was then subtracted from experimental absorbance spectra across the entire spectral region.

The spectral contribution of the protein in the near UV region (λ > 240 nm) was estimated by weighted summation (Gill et al., 1989; Pace et al., 1995) of the absorbance spectra of Tryptophan, Tyrosine and Phenylalanine (Mihalyi, 1968). As none of the 8 cysteine residues in the MenV N protein form disulphide bonds (Alayyoubi et al., 2015), no contribution from cystine groups is expected. A difference spectrum was obtained by subtracting the predicated protein absorbance spectrum from the absorbance spectrum of the NLPs. The spectra are reported in terms of the apparent molar absorption coefficient of the protein, ε (M^{-1} cm^{-1}) = A / (c (M) x l (cm)), where A is the absorbance, c is the protein concentration, and l is the optical path length.

For Circular Dichroism (CD) spectroscopy the NLPs were dialysed into a buffer containing 5 mM Na_2HPO_4/NaH_2PO_4 pH 7.0 and 100 mM NaF. The sample (1–15 µM final N protein concentration) was transferred into a 1 mm path length quartz cuvette (Hellma Analytics) and CD spectra (180–340 nm) collected at a temperature of 25 °C, using a Chirascan spectrophotometer (Applied Photophysics) with an optical bandwidth of 1 nm. Spectra were collected on the buffer alone, under

identical conditions. The averaged buffer spectrum was smoothed by fitting a LOESS model (Cleveland and Devlin, 1988) involving a second order polynomial. Smoothed buffer spectra were subtracted from the averaged sample spectra to yield the CD spectrum of the NLPs. The spectra are reported in terms of the apparent molar CD absorption coefficient of the protein, $\Delta\varepsilon$ (M^{-1} cm^{-1}) = ΔA / (c (M) x l (cm)), where ΔA is the differential absorbance of left and right circularly polarized light, c is the protein concentration, and l is the optical path length. No correction was made for circular differential light scattering (Tinoco et al., 1983) Given the large size of the NLPs this could potentially make a weak contribution to the CD signal at shorter wavelengths.

2.8. Inductively coupled mass spectrometry

An Agilent 7700 inductively coupled plasma-quadrupole mass spectrometer (ICP-QMS) was used to quantify the phosphorus content of the NLP sample. The signal was optimized by adjusting the power applied to the radio frequency coil. Analysis was run in Helium collision cell mode to reduce polyatomic interferences, by preventing interfering ions from entering the quadrupole mass analyser (Pröfrock et al., 2003; Vonderheide et al., 2003). Terbium was added as an internal standard, to monitor instrument stability. An inorganic phosphate solution (1000 ppm P stock, Peak Performance CPI international) was used to calibrate the instrument. This was diluted with ultrapure water to create a 6 ppm stock that was serially diluted with an acid matrix (10%(w/w) nitric acid, analytical grade) to make a range of element standards (3 ppm, 1.5 ppm, 1 ppm, 0.5 ppm, 0.1 ppm and 0.01 ppm).

To achieve optimal sensitivity NLP preparations were analysed at a total protein concentration of 20 mg/mL, to achieve the manufacturer recommended 0.05–0.3 ppm phosphorous content. Protein-containing solutions for analysis (70 µL) were added to 1900 µL of concentrated nitric acid (69%(w/w)), allowing for effective acid hydrolysis and dissolution of the nucleoprotein complex, then subsequently diluted to 10%(w/w) nitric acid with ultrapure water, prior to injection. Buffer only controls were treated in equivalent fashion. The presence of 0.25 mM TCEP.HCl in the buffer results in a small contribution to the total measured phosphorous content in the NLP preparation, and this was corrected for.

To calculate the RNA content of the NLPs, the phosphorous content in ppm was converted to total molar concentration of phosphorous. As RNA is the sole significant phosphorus source in the samples and there is one phosphorous atom per base, this is the equivalent of the molar nucleotide concentration. Division of the molar nucleotide concentration by the molar protein concentration then yields the nucleotide to protein ratio in the sample.

For control experiments, exploring the effects of the protein matrix on ICP-MS measurements, solid monophosphate ribonucleotides were dissolved in protein storage buffer (12.5 mM MOPS/KOH pH 7.0, 150 mM NaCl, 0.25 mM TCEP.HCl) and their concentration estimated using UV absorbance spectroscopy measurements at 260 nm (Cavaluzzi and Borer, 2004). An equimolar stock of all four ribonucleotides was prepared (9500 µM total concentration) and diluted to obtain standards for analysis at approximately; 0.75 ppm, 0.5 ppm, 0.1 ppm and 0.01 ppm total phosphorus, in the presence or absence of 20 g/L BSA (Merck, lyophilized protein). These samples were analysed as described above.

3. Results and discussion

3.1. Heterologous production of the Menangle Virus N protein, and the isolation of rings

Heterologous production of *Paramyxoviral* N proteins generates filamentous particles that are structurally indistinguishable from the viral nucleocapsid. These particles result from the non-specific

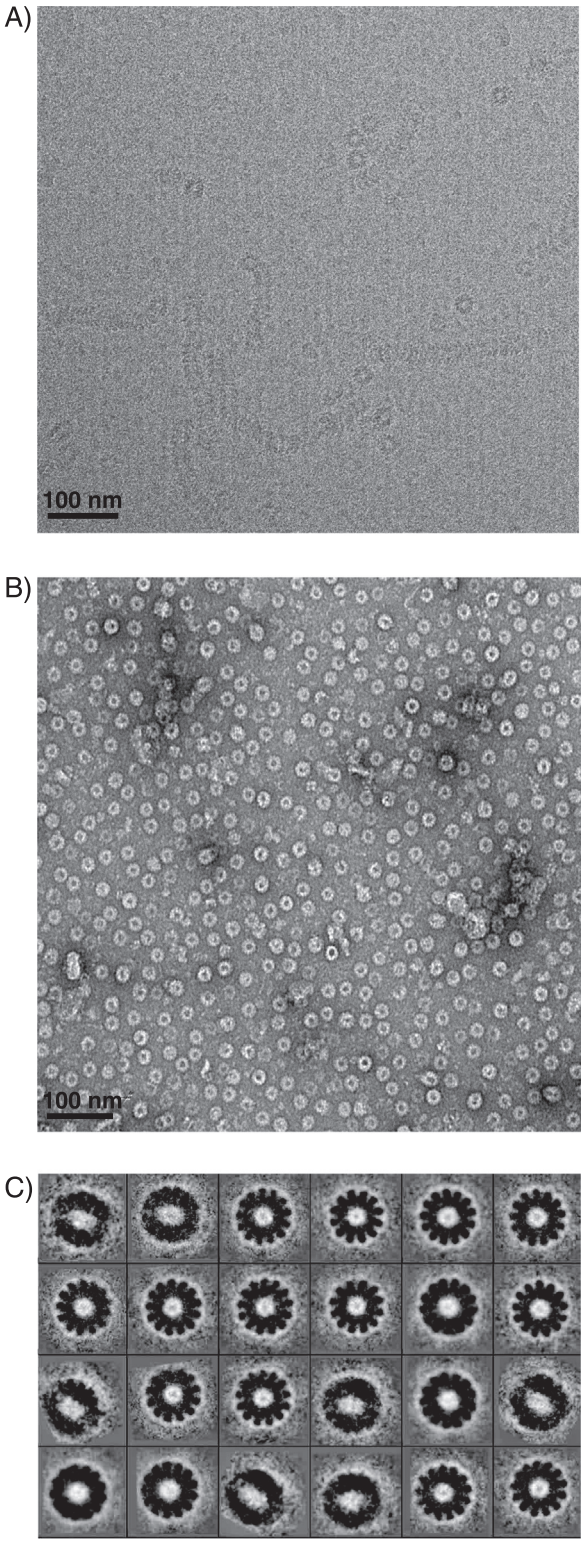

Fig. 1. Cryo-EM imaging of MenV NLPs. A) NLPs resulting from production of the MenV N protein in E. coli, before the isolation of rings. Filamentous structures of varying length are apparent, which closely resemble the authentic viral nucleocapsid. B) Purified MenV rings, modelling a single turn of the viral nucleocapsid C) 2D class averages of the rings, generated from ~9000 particle images. 13-fold cyclic symmetry is apparent in the class averaged images. A small number of particles were grouped in classes with 12-fold rotational symmetry (~280 particles) or classes in which the subunit geometry was not clearly defined (~615 particles).

packaging of cellular RNA (see, e.g. (Bhella et al., 2002; Fooks et al., 1993; Kingston et al., 2004; Samuel et al., 2002; Tan et al., 2004; Warnes et al., 1995)). Expression of the MenV N gene in *E. coli* generates NLPs (Fig. 1A) consistent with earlier expression studies in the yeast *S. cerevisiae* (Juozapaitis et al., 2007)

The filamentous NLPs have differing lengths, which can complicate biophysical and structural investigation. Hence we developed procedures to isolate rings, representing a single turn of the helical nucleocapsid. Structural analysis of the nucleocapsids of many non-segmented, single-stranded, negative-sense RNA viruses has rested on a similar approach (Alayyoubi et al., 2015; Albertini et al., 2006a, 2006b; Cox et al., 2009; Green et al., 2006; Iseni et al., 1998; Maclellan et al., 2007; Omari et al., 2008; Renner et al., 2016; Schoehn et al., 2001; Tawar et al., 2009). The lysis of bacterial cells by sonication helped to break down the helical NLPs, producing a mixture of rings and short helical filaments. A two-step ammonium sulphate precipitation then removed the bulk of the cellular contaminants. Subsequently size exclusion (Fig. S1) and anion exchange chromatography were used to separate rings from filaments. The exposure to high salt conditions during the ion exchange step also serves to remove any nucleic acids bound with low affinity.

Direct imaging of the purified NLPs using Cryo-electron microscopy (Cryo-EM) showed that rings predominate (Fig. 1B). In the thin layer of vitreous ice the particles were preferentially orientated such that only top views were observed (Fig. 1B), precluding single particle 3D reconstruction. However, class averaging of the 2D projection images could still be performed. In the majority of the 2D classes approximate 13-fold cyclic symmetry is apparent (Fig. 1C). Hence the MenV rings contain 13 N protein subunits, consistent with prior structural analysis on paramyxoviral nucleocapsids (Alayyoubi et al., 2015; Bhella et al., 2002, 2004; Cox et al., 2009; Desfosses et al., 2011; Egelman et al., 1989; Gutsche et al., 2015; Schoehn et al., 2004).

3.2. The total protein concentration can be estimated using the biuret assay

To estimate the total protein content in the ring preparation, we employed the colorimetric biuret assay. The biuret reaction involves binding of copper to the amide groups of the polypeptide backbone under highly alkaline conditions, to form a well characterized square-planar coordination complex (Freeman, 1967; Sigel and Martin, 1982). The purple-violet coloration associated with complex formation is followed spectrophotometrically at 550 nm. Based on the response of a pure protein standard of known concentration, the total protein concentration in an unknown can be reliably estimated (Rosenfeld, 1982; Sapan et al., 1999).

We employed the biuret assay because it exhibits little dependence on amino acid composition (see, e.g. (Bozimowski et al., 1983; Jenzano et al., 1986)) and there is no interference from nucleic acids. A variable response to different proteins is one of the principal problems besetting other colorimetric assays, such as the Lowry and bicinchoninic acid (BCA) assays (Peterson, 1979; Smith et al., 1985; Wiechelman et al., 1988), which amplify the signal from the biuret reaction, as well as the Bradford Dye binding assay (Kruger, 1994). Results from the biuret method are generally consistent with standard reference techniques for protein quantitation, such as Kjeldahl nitrogen determination (see, e.g. (Shrivastaw et al., 1995a, 1995b)).

One disadvantage of the biuret assay, which has contributed to its infrequent use, is relative insensitivity (Sapan et al., 1999). In practice, we found this was not limiting, and 50 µL samples containing 1.0 – 10 mg/mL protein could be readily analysed (Fig. S3). Our assay was based on the stable biuret reagent originally described by Weichselbaum (1946) and optimized by Gornall et al. (1949).

3.3. Biophysical analysis indicates the rings associate into double-ring discs in solution

Estimation of the protein concentration allowed for more detailed characterization of particle properties. Prior crystallographic analysis of the closely-related Parainfluenza virus 5 (PIV5) N protein had shown that 13-membered rings stack within the crystal via their “bottom” face, to form double-ring discs (Alayyoubi et al., 2015). Analogous stacking of the MenV rings in solution appeared likely, however this could not be inferred from the Cryo-EM images because of the absence of “side-views” (Fig. 1B). We therefore used hydrodynamic techniques to assess both the size and mass of the NLPs in solution.

The mean hydrodynamic radius (R_h) of the NLPs was determined using dynamic light scattering (DLS) (Fig. S4). When corrected to standard conditions (water at 20 °C) (van Holde, 1985) this yielded an estimate for the mean translational diffusion coefficient ($D_{20,w}$) of 1.677×10^{-11} m^2/s corresponding to a hydrodynamic radius (R_h) of 14.4 nm. This appears significantly larger than the hydrodynamic radius expected of either ring (7.7 nm) or disc (10.1 nm) – where the expected values are calculated for an appropriately dimensioned circular cylinder. However, this calculation neglects the effects of the intrinsically disordered tail of the N protein (aa 405–519) which would project from the surface of ring or disc, slowing diffusion and increasing the apparent size. In addition, even a minor population of helical filaments, which were occasionally observed by electron microscopy, would be heavily weighted in light scattering analysis. Hence the analysis was inconclusive, though the estimated polydispersity indicated that there was some size heterogeneity.

Sedimentation velocity AUC experiments were carried out to reliably determine the NLP mass distribution. Data were collected at three NLP concentrations (Fig. 2A) and analysed in SEDFIT to derive distributions of the sedimentation coefficient (Fig. 2B) and molar mass (Fig. 2C) (Dam and Schuck, 2004; Schuck, 2000). In the sedimentation coefficient distribution (Fig. 2B) a predominant species (~80%) with a sedimentation coefficient of 26 S is apparent, together with two minor species at 18 S (9%) and 40 S (12%).

The molar mass distribution (Fig. 2C) suggests that the most abundant species, at 26 S, corresponds to a double-ring disc (estimated molar mass 1430 kg/mol, expected molar mass 1560 kg/mol), while the minor species, at 18 S, corresponds to a single ring (estimated molar mass 818 kg/mol, expected molar mass 780 kg/mol). The variance between the estimated and expected masses may reflect the use of a single weight-average frictional ratio for all species in solution. For a sample with a multimodal sedimentation coefficient distribution (Fig. 2B), this approximation may impact the reliability of the mass estimates (Brown and Schuck, 2006). The broadly distributed minor species centred at 40 S most probably represents short helical filaments. Hence the NLP preparations contain a mixture of rings, discs and high mass species, with the predominant species being a disc, formed by two stacked rings.

We note that similar ring stacking occurs for the completely unrelated tobacco mosaic virus, and other filamentous plant viruses (Stubbs and Kendall, 2011). Although of no direct biological relevance, disc formation does have implications for in vitro biochemical and biophysical analysis of nucleocapsid function. It could, for example, occlude binding sites or alter access to bound nucleic acids.

3.4. Spectroscopic analysis confirms that the discs package nucleic acid

The packaging of nucleic acid by the MenV NLPs was confirmed using UV absorption and circular dichroism (CD) spectroscopy (Figs. 3 and 4).

The UV-absorbance spectra of nucleoprotein complexes are complicated by the overlapping absorption of protein and nucleic acid chromophores in the near UV region. For the NLP absorbance spectra, subtraction of the predicted protein contribution gave rise to a difference spectrum with the features expected of RNA (Voet et al., 1963)

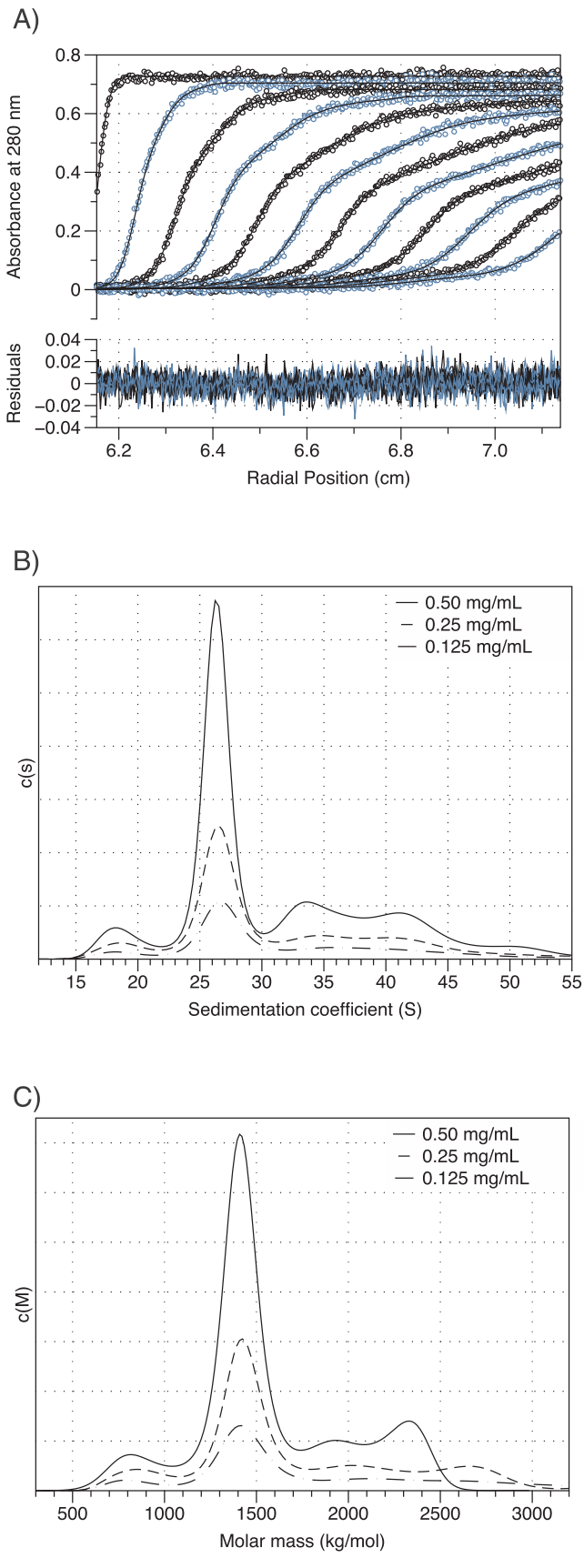

Fig. 2. Analytical ultracentrifugation indicates that double ring discs are the predominant species in solution. A) Sedimentation velocity analytical ultracentrifugation data and its direct modelling using the program SEDFIT. The top panel shows some time-dependent absorbance profiles of a sedimenting ring preparation, together with the fit model (every fifth scan is shown). The bottom panel shows the model residuals. B) Sedimentation coefficient distributions, c (s), show a predominant species with a sedimentation coefficient of 26 S. Minor species at 18 S and 40 S are also apparent C) Molar mass distributions, c(M), suggest that the major species is a double ring disc. The smaller species at 18 S has a mass corresponding to a single ring. The larger species, centred at 40 S, has a poorly defined mass and most probably corresponds to short helical filaments, which were not entirely eliminated during the purification process.

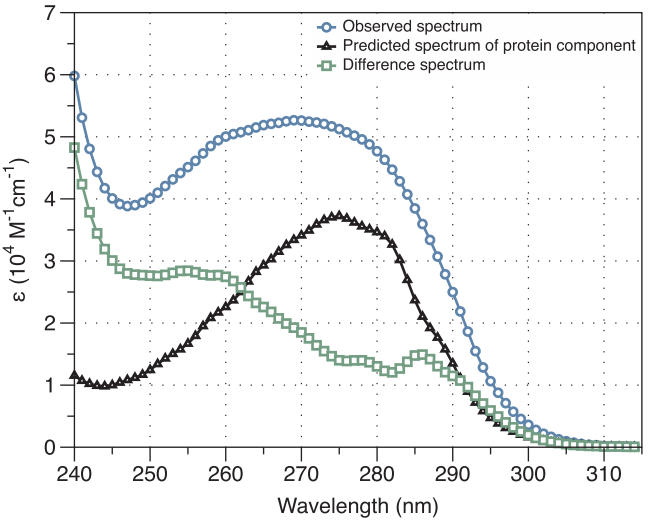

Fig. 3. UV absorbance spectra demonstrate that the particles package nucleic acids. The experimentally measured absorbance spectrum, following correction for light scattering, is shown in blue. The predicted absorbance spectrum of the protein component is shown in black. Subtraction of the predicted protein absorbance spectrum (black) from the NLP absorbance spectrum (blue) gives rise to a difference spectrum (green). This difference spectrum has the characteristics expected of nucleic acid, exhibiting steadily increasing absorbance at wavelengths < 300 nm and a local maximum at ~260 nm.

(Fig. 3).

Circular dichroism (CD) spectroscopy has the advantage that the spectral contributions of protein and nucleic acid are more effectively resolved. In the far UV region (λ < 250 nm), the CD spectrum of the NLPs (Fig. 4A) is dominated by the protein. The negative bands at 210 and 222 nm, and the positive band at 193 nm arise from the extensive α-helical secondary structure (45%) present within the Paramyxoviral N protein (Alayyoubi et al., 2015; Gutsche et al., 2015). In contrast, in the near UV region (Fig. 4B) the spectrum is dominated by the nucleic acid. The positive band between 250 and 300 nm originates from the bases of the bound RNA. Protein CD in this region is several orders of magnitude weaker, and has characteristic fine structure (Fasman, 1996; Martin and Schilstra, 2008). The near UV CD spectrum of the NLPs appears characteristic of ssRNA viruses (Piazzolla et al., 1986; Sokolova et al., 1982).

3.5. Quantification of bound nucleic acid using ICP-MS

The amount of RNA within MenV NLP preparations was quantified by determining the phosphorus content, using inductively coupled plasma mass spectrometry (ICP-MS). Phosphorus provides a unique elemental marker of the bound nucleic acids, so long as the protein is not itself significantly phosphorylated. While protein phosphorylation on serine, threonine, and tyrosine is not completely absent in bacteria, as was once thought (Macek and Mijakovic, 2011), it certainly occurs at

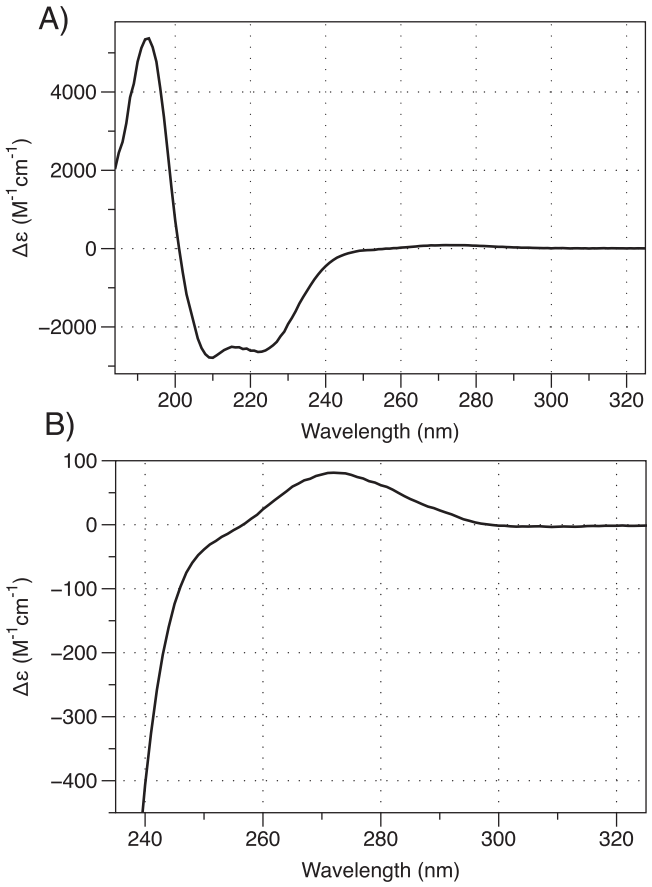

Fig. 4. Circular Dichroism spectra are consistent with RNA packaging. A) The far UV CD spectrum of the MenV NLPs is dominated by the protein contribution, and reflects the extensive alpha-helical secondary structure of the MenV N protein. The spectrum was collected at a low total N protein concentration (1 μM). B) The near UV CD spectrum of the MenV NLPs exhibits a weak positive band centred at 270 nm, characteristic of ssRNA viruses. This spectrum was collected with a higher total N protein concentration (10 μM) than the spectrum in A). Both the vertical and horizontal scales differ between panels A) and B).

much lower levels than in eukaryotic cells and employs a different repertoire of enzymes. The phosphorylation of heterologously produced proteins by the endogenous kinases of *E. coli* seems to occur only rarely (Sahdev et al., 2008; She et al., 2010). We note that the Menangle Virus N protein does not appear to be phosphorylated in mammalian cells (Shiell et al., 2002).

In ICP-MS atoms are ionized in the plasma and subsequently separated by their mass to charge ratio, before detection with a mass spectrometer. When using ICP-MS for phosphorus determination, the principle technical challenges arise from the element's high ionization potential, which results in relatively modest ionization efficiency in an argon plasma (Houk, 1986); the existence of a single stable isotope, which precludes the use of isotope dilution analysis; and the presence of interfering polyatomic ions that are generated in the ICP ion source, and complicate the spectra (Pröfrock et al., 2003; Wind et al., 2001). We found that the largest signal to background ratios were achieved with high power applied to the radio frequency coil. This elevates the plasma temperature, leading to increased phosphorus ionization (cf. (Kovačevič et al., 2004; Wuilloud et al., 2005)). Reduction of polyatomic interferences was achieved by running experiments in Helium collision cell mode (Donati et al., 2012; Pröfrock et al., 2003; Vonderheide et al., 2003). As an alternative, using an instrument equipped with a reaction cell it would be possible to generate the polyatomic ion $^{31}P^{16}O^{+}$ by reaction with oxygen gas (Bandura et al., 2002; Donati et al., 2012). The oxide ion, $^{31}P^{16}O^{+}$, is subject to less spectral interference than $^{31}P^{+}$.

To ensure efficient aerosolization, and as a precaution against clogging of the nebulizer, we added concentrated nitric acid to the sample prior to analysis, which will cause acid-catalysed hydrolysis of both proteins and nucleic acids (Brown, 1974; Hill, 1965). We subsequently diluted the sample to achieve a final working nitric acid concentration of ~10%(w/w). Direct addition of diluted nitric acid to the sample caused coagulation and precipitation of the ribonucleoprotein. We note that addition of nitric acid does not generate interferences, beyond those already arising from the air and water present in the sample.

To determine if there are protein matrix effects, which would impair the accuracy of the ICP-MS measurements, monophosphate ribonucleotides were analysed in the presence and absence of a protein standard. Across the concentration range analysed (0.7 − 51 μM monophosphate ribonucleotide, corresponding to 0.1–1.8 ppm phosphorous) the phosphorus content estimated using ICP-MS was unaffected by the presence or absence of BSA (20 mg/mL). This suggests that any matrix effects from protein are likely to be inconsequential. Furthermore, the phosphate content determined using ICP-MS, and the independently estimated nucleotide concentration determined using UV absorbance spectroscopy were linearly correlated (r^2 of 0.9998, data not shown), providing independent validation of the procedure.

Measurement of phosphorus content, combined with the independently determined total protein concentration, allowed calculation of the nucleotide / protein ratio in the NLP preparations. For three independent preparations, the molar ratio was determined to be 5.72 and 6.21 and 6.63 (Mean value 6.19, standard error of the mean 0.26). This is consistent with a large body of genetic, biochemical, and structural data showing that each paramyxoviral N protein can bind exactly 6 nucleotides of RNA (Alayyoubi et al., 2015; Calain and Roux, 1993; Gutsche et al., 2015; Kolakofsky et al., 1998). There are circumstances which would give rise to non-integer nucleotide-to-protein ratios. For example, the RNA present within the particles could be discontinuous and “gapped”, or the minor population of filaments present could be carrying an overhanging stub of RNA. However, given the precision of our estimate, the most straightforward interpretation is that the MenV NLPs are fully loaded with nucleic acid.

4. Conclusion

While a variety of procedures have been developed for estimating the protein and nucleic acid content of nucleoprotein complexes from UV absorbance measurements (Groves et al., 1968; Mach et al., 1992; Porterfield and Zlotnick, 2010; Wilson et al., 1989), all involve some approximation, and application to particles containing structured nucleic acids may be problematic. Here we have suggested an alternative approach, which rests on the quantification of phosphorus contributed by the nucleic acids, coupled with the independent determination of the protein content.

The method could be streamlined if suitable instrumentation were available. In a nucleoprotein complex, the element sulphur (S), is unique to the protein side chains of cysteine and methionine. Using ICP-MS to quantify both sulphur and phosphorus would therefore determine both the protein and nucleic acid content in the sample, eliminating the need for the biuret assay. Similar to phosphorous, the determination of sulphur using ICP-MS is complicated by a low ionization potential, and the presence of interfering polyatomic ions. Procedures have been developed that allow the simultaneous determination of both P and S, by production of oxide ions $^{31}P^{16}O^{+}$ and $^{32}S^{16}O^{+}$, respectively (Bandura et al., 2002; Ciavardelli et al., 2010; Gong et al., 2015; Thompson et al., 2013). However for optimal sensitivity these experiments require instruments equipped with a dynamic reaction and collision cell (Ciavardelli et al., 2010), which at present are less widely available than the simple quadrupole based ICP-MS system used in this work.

ICP-MS has established utility for the analysis of protein

phosphorylation (Ciavardelli et al., 2010; Navaza et al., 2007). We suggest that the same technique can be routinely used for compositional analysis of recombinant nucleoprotein complexes, in situations where protein phosphorylation is likely to be insignificant.

Acknowledgements

We thank Mr Stuart Morrow (Auckland Mass Spectrometry Centre) for assistance with the ICP-MS measurements, Dr David Goldstone for advice on Analytical Ultracentrifugation, and Dr Adrian Turner (Auckland Imaging Centre) and Dr Ambroise Desfosses for assistance with electron microscopy. This work was funded by a RSNZ Marsden grant (UOA1202).

Appendix A. Supporting information

Supplementary data associated with this article can be found in the online version at doi:10.1016/j.virol.2018.11.013.

References

Alayyoubi, M., Leser, G.P., Kors, C.A., Lamb, R.A., 2015. Structure of the paramyxovirus parainfluenza virus 5 nucleoprotein-RNA complex. Proc. Natl. Acad. Sci. USA 112, E1792–E1799. https://doi.org/10.1073/pnas.1503941112.

Albertini, A.A.V., Clapier, C.R., Wernimont, A.K., Schoehn, G., Weissenhorn, W., Ruigrok, R.W.H., 2006a. Isolation and crystallization of a unique size category of recombinant Rabies virus Nucleoprotein-RNA rings. J. Struct. Biol. 158, 129–133. https://doi.org/10.1016/j.jsb.2006.10.011.

Albertini, A.A.V., Wernimont, A.K., Muziol, T., Ravelli, R.B.G., Clapier, C.R., Schoehn, G., Weissenhorn, W., Ruigrok, R.W.H., 2006b. Crystal structure of the rabies virus nucleoprotein-RNA complex. Science 313, 360–363. https://doi.org/10.1126/science.1125280.

Bandura, D.R., Baranev, V.I., Tanner, S.D., 2002. Detection of ultratrace phosphorus and sulfur by quadrupole ICPMS with dynamic reaction cell. Anal. Chem. 74, 1497–1502. https://doi.org/10.1021/ac011031v.

Bárcena, J., Blanco, E., 2013. Design of Novel Vaccines Based on Virus-Like Particles or Chimeric Virions. In: Mateu, M.G. (Ed.), Structure and Physics of Viruses, Subcellular Biochemistry. Springer, Netherlands, Dordrecht, pp. 631–665. https://doi.org/10.1007/978-94-007-6552-8_21.

Bhella, D., Ralph, A., Murphy, L.B., Yeo, R.P., 2002. Significant differences in nucleocapsid morphology within the Paramyxoviridae. J. Gen. Virol. 83, 1831–1839.

Bhella, D., Ralph, A., Yeo, R.P., 2004. Conformational flexibility in recombinant measles virus nucleocapsids visualised by cryo-negative stain electron microscopy and real-space helical reconstruction. J. Mol. Biol. 340, 319–331. https://doi.org/10.1016/j.jmb.2004.05.015.

Bittner, A.M., Alonso, J.M., Górzny, M.Ł., Wege, C., 2013. Nanoscale Science and Technology with Plant Viruses and Bacteriophages. In: Mateu, M.G. (Ed.), Structure and Physics of Viruses, Subcellular Biochemistry. Springer, Netherlands, Dordrecht, pp. 667–702. https://doi.org/10.1007/978-94-007-6552-8_22.

Bloomfield, V.A., Crothers, D.M., Tinoco, I., J., 2000. Nucleic Acids. University Science Books.

Bowden, T.R., Westenberg, M., Wang, L.-F., Eaton, B.T., Boyle, D.B., 2001. Molecular characterization of Menangle virus, a novel paramyxovirus which infects pigs, fruit bats, and humans. Virology 283, 358–373. https://doi.org/10.1006/viro.2001.0893.

Bozimowski, D., Artiss, J.D., Zak, B., 1983. Spectrophotometric comparison of several reactions used for cerebrospinal fluid protein determinations. Microchem. J. 28, 285–293. https://doi.org/10.1016/0026-265X(83)90060-7.

Briggs, J.A.G., Simon, M.N., Gross, I., Krausslich, H.-G., Fuller, S.D., Vogt, V.M., Johnson, M.C., 2004. The stoichiometry of Gag protein in HIV-1. Nat. Struct. Mol. Biol. 11, 672–675. https://doi.org/10.1038/nsmb785.

Brown, D.M., 1974. Chemical Reactions of Polynucleotides And Nucleic Acids. In: Ts'o, Paul O.P. (Ed.), Basic Principles in Nucleic Acid Chemistry Volume II. ACADEMIC PRESS, INC, pp. 1–90. https://doi.org/10.1016/B978-0-12-701902-4.50007-1.

Brown, P.H., Schuck, P., 2006. Macromolecular size-and-shape distributions by sedimentation velocity analytical ultracentrifugation. Biophys. J. 90, 4651–4661. https://doi.org/10.1529/biophysj.106.081372.

Bruzzesi, M.R., Chiancone, E., Antonini, E., 1965. Association-dissociation properties of lysozyme. Biochemistry 4, 1796–1800. https://doi.org/10.1021/bi00885a016.

Calain, P., Roux, L., 1993. The rule of six, a basic feature for efficient replication of Sendai virus defective interfering RNA. J. Virol. 67, 4822–4830.

Camerini-Otero, R., Day, L., 1978. Wavelength dependence of turbidity of solutions of macromolecules. Biopolymers 17, 2241–2249.

Candiano, G., Bruschi, M., Musante, L., Santucci, L., Ghiggeri, G.M., Carnemolla, B., Orecchia, P., Zardi, L., Righetti, P.G., 2004. Blue silver: a very sensitive colloidal Coomassie G-250 staining for proteome analysis. Electrophoresis 25, 1327–1333. https://doi.org/10.1002/elps.200305844.

Carrico, I.S., Kirshenbaum, K., 2009. Nanoparticles: designer labels for virus coats. Nat. Nanotechnol. 4, 14–15. https://doi.org/10.1038/nnano.2008.389.

Cavaluzzi, M.J., Borer, P.N., 2004. Revised UV extinction coefficients for nucleoside-5′-monophosphates and unpaired DNA and RNA. Nucleic Acids Res. 32, e13. https://doi.org/10.1093/nar/gnh015.

Ciavardelli, D., Sacchetta, P., Federici, G., Di Ilio, C., Urbani, A., 2010. Protein phosphorylation stoichiometry by simultaneous ICP-QMS determination of phosphorus and sulfur oxide ions: a multivariate optimization of plasma operating conditions. Talanta 80, 1513–1525. https://doi.org/10.1016/j.talanta.2009.06.082.

Cleveland, W.S., Devlin, S.J., 1988. Locally weighted regression - an approach to regression-analysis by local fitting. J. Am. Stat. Assoc. 83, 596–610.

Cox, R., Green, T.J., Qiu, S., Kang, J., Tsao, J., Prevelige Jr, P.E., He, B., Luo, M., 2009. Characterization of a mumps virus nucleocapsidlike particle. J. Virol. 83, 11402–11406. https://doi.org/10.1128/JVI.00504-09.

Cuervo, A., Daudén, M.I., Carrascosa, J.L., 2013. Nucleic Acid Packaging in Viruses. In: Mateu, M.G. (Ed.), Structure and Physics of Viruses, Subcellular Biochemistry. Springer, Netherlands, Dordrecht, pp. 361–394. https://doi.org/10.1007/978-94-007-6552-8_12.

Dam, J., Schuck, P., 2004. Calculating sedimentation coefficient distributions by direct modeling of sedimentation velocity concentration profiles. Meth Enzymol. 384, 185–212. https://doi.org/10.1016/S0076-6879(04)84012-6.

Desfosses, A., Goret, G., Farias Estrozi, L., Ruigrok, R.W.H., Gutsche, I., 2011. Nucleoprotein-RNA orientation in the measles virus nucleocapsid by three-dimensional electron microscopy. J. Virol. 85, 1391–1395. https://doi.org/10.1128/JVI.01459-10.

Donati, G.L., Amais, R.S., Nóbrega, J.A., 2012. Strategies to improve accuracy and sensitivity in phosphorus determinations by inductively coupled plasma quadrupole mass spectrometry. J. Braz. Chem. Soc. 23, 786–791. https://doi.org/10.1590/S0103-50532012000400026.

Dubochet, J., Ducommun, M., Zollinger, M., Kellenberger, E., 1971. A new preparation method for dark-field electron microscopy of biomacromolecules. J. Ultrastruct. Res. 35, 147–167. https://doi.org/10.1016/S0022-5320(71)80148-X.

Duong-Ly, K.C., Gabelli, S.B., 2014. Salting out of proteins using ammonium sulfate precipitation. Meth. Enzymol. 541, 85–94. https://doi.org/10.1016/B978-0-12-420119-4.00007-0.

Durchschlag, H., 1989. Determination of the partial specific volume of conjugated proteins. Colloid Polym. Sci. 267, 1139–1150.

Egelman, E.H., Wu, S.S., Amrein, M., Portner, A., Murti, G., 1989. The Sendai virus nucleocapsid exists in at least four different helical states. J. Virol. 63, 2233–2243.

Englard, S., Seifter, S., 1990. Precipitation techniques. Meth. Enzymol. 182, 285–300. https://doi.org/10.1016/0076-6879(90)82024-V.

Fasman, G.D., 1996. Circular Dichroism and the Conformational Analysis of BioMolecules. Springer.

Ferrer, M., Henriet, S., Chamontin, C., Lainé, S., Mougel, M., 2016. From cells to virus particles: quantitative methods to monitor RNA packaging. Viruses 8, 239. https://doi.org/10.3390/v8080239.

Finsy, R., De Jaeger, N., 1991. Particle sizing by photon correlation spectroscopy. Part II: average values. Part. Part. Syst. Charact. 8, 187–193.

Fooks, A.R., Stephenson, J.R., Warnes, A., Dowsett, A.B., Rima, B.K., Wilkinson, G.W., 1993. Measles virus nucleocapsid protein expressed in insect cells assembles into nucleocapsid-like structures. J. Gen. Virol. 74 (Pt 7), 1439–1444. https://doi.org/10.1099/0022-1317-74-7-1439.

Freeman, H.C., 1967. Crystal structures of metal-peptide complexes. Adv. Protein Chem. 22, 257–424. https://doi.org/10.1016/S0065-3233(08)60043-1.

Frisken, B.J., 2001. Revisiting the method of cumulants for the analysis of dynamic light-scattering data. Appl. Opt. 40, 4087–4091.

Gill, S.C., Hippel, von, P.H., 1989. Calculation of protein extinction coefficients from amino acid sequence data. Anal. Biochem. 182, 319–326.

Gong, J., Solivio, M.J., Merino, E.J., Caruso, J.A., Landero-Figueroa, J.A., 2015. Developing ICP-MS/MS for the detection and determination of synthetic DNA-protein crosslink models via phosphorus and sulfur detection. Anal. Bioanal. Chem. 407, 2433–2437. https://doi.org/10.1007/s00216-015-8504-x.

Gornall, A.G., Manolis, A., 1977. Comments on a new biuret reagent. Clin. Chem. 23, 1184–1185.

Gornall, A.G., Bardawill, C.J., David, M.M., 1949. Determination of serum proteins by means of the biuret reaction. J. Biol. Chem. 177, 751–766.

Green, T.J., Zhang, X., Wertz, G.W., Luo, M., 2006. Structure of the vesicular stomatitis virus nucleoprotein-RNA complex. Science 313, 357–360. https://doi.org/10.1126/science.1126953.

Groves, W.E., Davis, F.C., Sells, B.H., 1968. Spectrophotometric determination of microgram quantities of protein without nucleic acid interference. Anal. Biochem. 22, 195–210. https://doi.org/10.1016/0003-2697(68)90307-2.

Gutsche, I., Desfosses, A., Effantin, G., Ling, W.L., Haupt, M., Ruigrok, R.W.H., Sachse, C., Schoehn, G., 2015. Structural virology. Near-atomic cryo-EM structure of the helical measles virus nucleocapsid. Science 348, 704–707. https://doi.org/10.1126/science.aaa5137.

Hansen, S., 2004. Translational friction coefficients for cylinders of arbitrary axial ratios estimated by Monte Carlo simulation. J. Chem. Phys. 121, 9111–9115. https://doi.org/10.1063/1.1803533.

Harding, S.E., 1994. Determination of diffusion coefficients of biological macromolecules by dynamic light scattering. Methods Mol. Biol. 22, 97–108.

Harding, S.E., 1986. Applications of light scattering in microbiology. Biotechnol. Appl. Biochem. 8, 489–509.

Hill, R.L., 1965. Hydrolysis of proteins. Adv. Protein Chem. 20, 37–107. https://doi.org/10.1016/S0065-3233(08)60388-5.

Honn, K.V., Chavin, W., 1975. An improved automated Biuret method for the determination of microgram protein concentrations. Anal. Biochem 68, 230–235.

Houk, R.S., 1986. Mass spectrometry of inductively coupled plasmas. Anal. Chem. 58, 97A–105A. https://doi.org/10.1021/ac00292a788.

Iseni, F., Barge, A., Baudin, F., Blondel, D., Ruigrok, R.W.H., 1998. Characterization of rabies virus nucleocapsids and recombinant nucleocapsid-like structures. J. Gen. Virol. 79, 2909–2919. https://doi.org/10.1099/0022-1317-79-12-2909.

Jenzano, J.W., Hogan, S.L., Noyes, C.M., Featherstone, G.L., Lundblad, R.L., 1986. Comparison of five techniques for the determination of protein content in mixed human saliva. Anal. Biochem. 159, 370–376. https://doi.org/10.1016/0003-2697(86)90355-6.

Juozapaitis, M., Serva, A., Kucinskaite, I., Zvirbliene, A., Slibinskas, R., Staniulis, J., Sasnauskas, K., Shiell, B.J., Bowden, T.R., Michalski, W.P., 2007. Generation of Menangle virus nucleocapsid-like particles in yeast Saccharomyces cerevisiae. J. Biotechnol. 130, 441–447. https://doi.org/10.1016/j.jbiotec.2007.05.013.

Kingston, R.L., Baase, W.A., Gay, L.S., 2004. Characterization of nucleocapsid binding by the measles virus and mumps virus phosphoproteins. J. Virol. 78, 10097. https://doi.org/10.1128/JVI.78.16.8630-8640.2004.

Kolakofsky, D., Pelet, T., Garcin, D., Hausmann, S., Curran, J., Roux, L., 1998. Paramyxovirus RNA synthesis and the requirement for hexamer genome length: the rule of six revisited. J. Virol. 72, 891–899.

Koppel, D.E., 1972. Analysis of macromolecular polydispersity in intensity correlation spectroscopy: the method of cumulants. J. Chem. Phys. 57, 4814–4820. https://doi.org/10.1063/1.1678153.

Kovačevič, M., Leber, R., Kohlwein, S.D., Goessler, W., 2004. Application of inductively coupled plasma mass spectrometry to phospholipid analysis. J. Anal. At. Spectrom. 19, 80–84. https://doi.org/10.1039/b307545a.

Kruger, N.J., 1994. The Bradford method for protein quantitation. Methods Mol. Biol. 32, 9–15. https://doi.org/10.1385/0-89603-268-X:9.

Laue, T.M., Shah, B.D., Ridgeway, T.M., Pelletier, S.L., 1992. Computer-aided interpretation of analytical sedimentation data for proteins, In: Harding, S.E., Rowe, A.J., Horton, J.C. (Eds.), Analytical Ultracentrifugation in Biochemistry and Polymer Science.

Losen, M., Frölich, B., Pohl, M., Büchs, J., 2004. Effect of oxygen limitation and medium composition on Escherichia coli fermentation in shake-flask cultures. Biotechnol. Prog. 20, 1062–1068. https://doi.org/10.1021/bp034282t.

Macek, B., Mijakovic, I., 2011. Site-specific analysis of bacterial phosphoproteomes. Proteomics 11, 3002–3011. https://doi.org/10.1002/pmic.201100012.

Mach, H., Middaugh, C.R., Lewis, R.V., 1992. Detection of proteins and phenol in DNA samples with second-derivative absorption spectroscopy. Anal. Biochem. 200, 20–26.

Maclellan, K., Loney, C., Yeo, R.P., Bhella, D., 2007. The 24A structure of Respiratory Syncytial Virus N-RNA decameric rings. J. Virol. 81, 9519–9524. https://doi.org/10.1128/JVI.00526-07.

Martin, S.R., Schilstra, M.J., 2008. Circular dichroism and its application to the study of biomolecules. Methods Cell Biol. 84, 263–293. https://doi.org/10.1016/S0091-679X(07)84010-6.

Mihalyi, E., 1968. Numerical values of the absorbances of the aromatic amino acids in acid, neutral, and alkaline solutions. J. Chem. Eng. Data 13, 179–182.

Müller, S.A., Müller, D.J., Engel, A., 2011. Assessing the structure and function of single biomolecules with scanning transmission electron and atomic force microscopes. Micron 42, 186–195. https://doi.org/10.1016/j.micron.2010.10.002.

Narayanan, K.B., Han, S.S., 2017. Helical plant viral nanoparticles-bioinspired synthesis of nanomaterials and nanostructures. Bioinspir. Biomim. 12, 031001. https://doi.org/10.1088/1748-3190/aa6bfd.

Navaza, A.P., Encinar, J.R., Sanz-Medel, A., 2007. Quantitative protein phosphorylation analysis: the role of ICP-MS. J. Anal. At. Spectrom. 22, 1223–1237. https://doi.org/10.1039/B703555A.

Omari, El, K., Scott, K., Dhaliwal, B., Ren, J., Abrescia, N.G.A., Budworth, J., Lockyer, M., Powell, K.L., Hawkins, A.R., Stammers, D.K., 2008. Crystallization and preliminary X-ray analysis of the human respiratory syncytial virus nucleocapsid protein. Acta Crystallogr. F 64, 1019–1023. https://doi.org/10.1107/S1744309108031059.

Pace, C.N., Vajdos, F., Fee, L., Grimsley, G., Gray, T., 1995. How to measure and predict the molar absorption coefficient of a protein. Protein Sci. 4, 2411–2423.

Peterson, G.L., 1979. Review of the Folin phenol protein quantitation method of Lowry, Rosebrough, Farr and Randall. Anal. Biochem. 100, 201–220. https://doi.org/10.1016/0003-2697(79)90222-7.

Piazzolla, P., Guantieri, V., Tamburro, A.M., 1986. Spectroscopic studies on purified particles and isolated RNA of cucumber mosaic virus. J. Gen. Virol. 67, 69–74. https://doi.org/10.1099/0022-1317-67-1-69.

Porterfield, J.Z., Zlotnick, A., 2010. A simple and general method for determining the protein and nucleic acid content of viruses by UV absorbance. Virology 407, 281–288. https://doi.org/10.1016/j.virol.2010.08.015.

Pröfrock, D., Leonhard, P., Prange, A., 2003. Determination of phosphorus in phosphorylated deoxyribonucleotides using capillary electrophoresis and high performance liquid chromatography hyphenated to inductively coupled plasma mass spectrometry with an octopole reaction cell. J. Anal. At. Spectrom. 18, 708–713. https://doi.org/10.1039/B302445H.

Renner, M., Bertinelli, M., Leyrat, C., Paesen, G.C., Saraiva de Oliveira, L.F., Huiskonen, J.T., Grimes, J.M., 2016. Nucleocapsid assembly in pneumoviruses is regulated by conformational switching of the N protein. eLife 5, e12627. https://doi.org/10.7554/eLife.12627.

Reynolds, J.A., Nozaki, Y., Tanford, C., 1983. Gel-exclusion chromatography on S1000 Sephacryl: application to phospholipid vesicles. Anal. Biochem. 130, 471–474.

Roldão, A., Mellado, M.C.M., Castilho, L.R., Carrondo, M.J.T., Alves, P.M., 2010. Virus-like particles in vaccine development. Expert Rev. Vaccin. 9, 1149–1176. https://doi.org/10.1586/erv.10.115.

Rosenfeld, L., 1982. In: Origins of Clinical Chemistry. ACADEMIC PRESS, INC, pp. 113–143. https://doi.org/10.1016/B978-0-12-597580-3.50017-3.

Ruigrok, R.W.H., Crépin, T., Kolakofsky, D., 2011. Nucleoproteins and nucleocapsids of negative-strand RNA. viruses, Curr. Opin. Microbiol. 14, 504–510. https://doi.org/10.1016/j.mib.2011.07.011.

Sahdev, S., Khattar, S.K., Saini, K.S., 2008. Production of active eukaryotic proteins through bacterial expression systems: a review of the existing biotechnology strategies. Mol. Cell. Biochem. 307, 249–264. https://doi.org/10.1007/s11010-007-9603-6.

Samuel, D., Sasnauskas, K., Jin, L., Beard, S., Zvirbliene, A., Gedvilaite, A., Cohen, B., 2002. High level expression of recombinant mumps nucleoprotein in Saccharomyces cerevisiae and its evaluation in mumps IgM serology. J. Med. Virol. 66, 123–130. https://doi.org/10.1002/jmv.2120.

Sapan, C.V., Lundblad, R.L., Price, N.C., 1999. Colorimetric protein assay techniques. Biotechnol. Appl. Biochem. 29 (Pt 2), 99–108.

Schneemann, A., 2006. The structural and functional role of RNA in icosahedral virus assembly. Annu. Rev. Microbiol. 60, 51–67. https://doi.org/10.1146/annurev.micro.60.080805.142304.

Schoehn, G., Iseni, F., Mavrakis, M., Blondel, D., Ruigrok, R.W.H., 2001. Structure of recombinant rabies virus nucleoprotein-RNA complex and identification of the phosphoprotein binding site. J. Virol. 75, 490–498. https://doi.org/10.1128/JVI.75.1.490-498.2001.

Schoehn, G., Mavrakis, M., Albertini, A., Wade, R., Hoenger, A., Ruigrok, R.W.H., 2004. The 12 A structure of trypsin-treated measles virus N-RNA. J. Mol. Biol. 339, 301–312. https://doi.org/10.1016/j.jmb.2004.03.073.

Schuck, P., 2000. Size-distribution analysis of macromolecules by sedimentation velocity ultracentrifugation and Lamm equation modeling. Biophys. J. 78, 1606–1619. https://doi.org/10.1016/S0006-3495(00)76713-0.

She, Y.-M., Xu, X., Yakunin, A.F., Dhe-Paganon, S., Donald, L.J., Standing, K.G., Lee, D.C., Jia, Z., Cyr, T.D., 2010. Mass spectrometry following mild enzymatic digestion reveals phosphorylation of recombinant proteins in Escherichia coli through mechanisms involving direct nucleotide binding. J. Proteome Res. 9, 3311–3318. https://doi.org/10.1021/pr9011987.

Shiell, B.J., Beddome, G., Michalski, W.P., 2002. Mass spectrometric identification and characterisation of the nucleocapsid protein of Menangle virus. J. Virol. Methods 102, 27–35. https://doi.org/10.1016/S0166-0934(01)00441-4.

Shrivastaw, K.P., Jhamb, S.S., Kumar, A., 1995a. Quantitation of the protein-content of diphtheria and tetanus toxoids by the biuret method during production of combined vaccines. Biologicals 23, 61–63. https://doi.org/10.1016/1045-1056(95)90013-6.

Shrivastaw, K.P., Singh, S., Sharma, S.B., Sokhey, J., 1995b. Quantitation of protein content by biuret method during production of yellow fever vaccine. Biologicals 23, 299–300. https://doi.org/10.1006/biol.1995.0048.

Sigel, H., Martin, R.B., 1982. Coordinating properties of the amide bond. stability and structure of metal ion complexes of peptides and related ligands. Chem. Rev. 82, 385–426. https://doi.org/10.1021/cr00050a003.

Smith, P.K., Krohn, R.I., Hermanson, G.T., Mallia, A.K., Gartner, F.H., Provenzano, M.D., Fujimoto, E.K., Goeke, N.M., Olson, B.J., Klenk, D.C., 1985. Measurement of protein using bicinchoninic acid. Anal. Biochem. 150, 76–85. https://doi.org/10.1016/0003-2697(85)90442-7.

Sokolova, M.V., Yaroslavtseva, N.G., Kharitonenkov, I.G., Khristova, M.L., 1982. An investigation of influenza virus ribonucleoprotein structure by means of circular dichroism. Mol. Biol. (Moscow, Russ. Fed., Engl. Ed.) 16, 47–52.

Stubbs, G., Kendall, A., 2011. Helical Viruses. In: Rossmann, M.G., Rao, V.B. (Eds.), Viral Molecular Machines, Advances in Experimental Medicine and Biology. Springer, US, Boston, MA, pp. 631–658. https://doi.org/10.1007/978-1-4614-0980-9_28.

Tan, W.S., Ong, S.T., Eshaghi, M., Foo, S.-S., Yusoff, K., 2004. Solubility, immunogenicity and physical properties of the nucleocapsid protein of Nipah virus produced in Escherichia coli. J. Med. Virol. 73, 105–112. https://doi.org/10.1002/jmv.20052.

Tang, G., Peng, L., Baldwin, P.R., Mann, D.S., Jiang, W., Rees, I., Ludtke, S.J., 2007. EMAN2: an extensible image processing suite for electron microscopy. J. Struct. Biol. 157, 38–46. https://doi.org/10.1016/j.jsb.2006.05.009.

Tawar, R.G., Duquerroy, S., Vonrhein, C., Varela, P.F., Damier-Piolle, L., Castagné, N., Maclellan, K., Bedouelle, H., Bricogne, G., Bhella, D., Eléouët, J.-F., Rey, F.A., 2009. Crystal structure of a nucleocapsid-like nucleoprotein-RNA complex of respiratory syncytial virus. Science 326, 1279–1283. https://doi.org/10.1126/science.1177634.

Thomas, D., Schultz, P., Steven, A.C., Wall, J.S., 1994. Mass analysis of biological macromolecular complexes by STEM. Biol. Cell 80, 181–192.

Thompson, D.F., Michopoulos, F., Smith, C.J., Duckett, C.J., Wilkinson, R.W., Jarvis, P., Wilson, I.D., 2013. Phosphorus and sulfur metabonomic profiling of tissue and plasma obtained from tumour-bearing mice using ultra-performance liquid chromatography/ inductively coupled plasma mass spectrometry. Rapid Commun. Mass Spectrom. 27, 2539–2545. https://doi.org/10.1002/rcm.6722.

Tinoco, I., Maestre, M.F., Bustamante, C., 1983. Circular dichroism in samples which scatter light. Trends Biochem. Sci. 8, 41–44. https://doi.org/10.1016/0968-0004(83)90379-1.

van Holde, K., 1985. Physical Biochemistry, 2nd ed. Prentice-Hall.

Voet, D., Gratzer, W.B., Cox, R.A., Doty, P., 1963. Absorption spectra of nucleotides, polynucleotides, and nucleic acids in the far ultraviolet. Biopolymers 1, 193–208. https://doi.org/10.1002/bip.360010302.

Vonderheide, A.P., Meija, J., Montes-Bayón, M., Caruso, J.A., 2003. Use of optional gas and collision cell for enhanced sensitivity of the organophosphorus pesticides by GC-ICP-MS. J. Anal. At. Spectrom. 18, 1097–1102. https://doi.org/10.1039/b301704d.

Warnes, A., Fooks, A.R., Dowsett, A.B., Wilkinson, G.W., Stephenson, J.R., 1995. Expression of the measles virus nucleoprotein gene in Escherichia coli and assembly of nucleocapsid-like structures. Gene 160, 173–178.

Weichselbaum, C.T.E., 1946. An accurate and rapid method for the determination of proteins in small amounts of blood serum and plasma. Am. J. Clin. Pathol. 16, 40–49. https://doi.org/10.1093/ajcp/16.3_ts.40.

Wiechelman, K.J., Braun, R.D., Fitzpatrick, J.D., 1988. Investigation of the bicinchoninic acid protein assay: identification of the groups responsible for color formation. Anal.

Biochem. 175, 231–237. https://doi.org/10.1016/0003-2697(88)90383-1.
Wilson, C., Matthews, F., Greasham, R.L., Will, M., Copeland, R.A., 1989. Application of fourth derivative absorption spectroscopy to protein quantitation during purification. Anal. Biochem. 182, 141–145.
Wind, M., Wesch, H., Lehmann, W.D., 2001. Protein phosphorylation degree: determination by capillary liquid chromatography and inductively coupled plasma mass spectrometry. Anal. Chem. 73, 3006–3010. https://doi.org/10.1021/ac010066s.
Wuilloud, R.G., Shah, M., Kannamkumarath, S.S., Altamirano, J.C., 2005. The potential of inductively coupled plasma-mass spectrometric detection for capillary electrophoretic analysis of pesticides. Electrophoresis 26, 1598–1605. https://doi.org/10.1002/elps.200410098.
Yegambaram, K., Bulloch, E.M.M., Kingston, R.L., 2013. Protein domain definition should allow for conditional disorder. Protein Sci. 22, 1502–1518. https://doi.org/10.1002/pro.2336.
Zeltins, A., 2013. Construction and characterization of virus-like particles: a review. Mol. Biotechnol. 53, 92–107. https://doi.org/10.1007/s12033-012-9598-4.